Lightly Damped Moment-Resisting Steel Frames: A Design-Based Approach

OZGUR ATLAYAN and FINLEY A. CHARNEY

ABSTRACT

The current U.S. seismic design provisions for steel moment-resisting frames generally result in structures for which stiffness is the controlling factor in the design. The design for stiffness often provides considerable overstrength, which reduces rotational ductility demand on the plastic hinges in the structure. Even though the reduction in ductility demand may be considerable, the design provisions do not allow the detailing rules to be waived, resulting in designs that may not be economically optimized. This paper presents the results of a study in which a variety of steel frames were designed for strength and that used added energy dissipation in the form of linear viscous dampers to control the drift. The goal of the study was to provide only enough damping to control the drift, and to this end, it was found that total system damping of 10% critical was sufficient. As shown in the paper, the added damping provided the required drift control and had the added advantage of minimizing the dispersion, which typically occurs in response history analyses carried out under several appropriately scaled ground motions. Such dispersion control is illustrated through incremental dynamic analysis of damped nine-story buildings in Seattle, Washington.

Keywords: seismic design and performance, viscous fluid dampers, incremental dynamic analysis.

Properly designed moment-resisting steel frames are generally very effective in resisting strong earthquakes. However these systems, designed for strength alone, may not have sufficient stiffness to meet drift or stability limits. Increasing the stiffness increases the strength, and theoretically, the increased strength would reduce the ductility demands. If the ductility demands were reduced enough, it would seem feasible to relax the detailing requirements, and possibly, enhance the economy of the system. Current U.S. design provisions such as the 2005 AISC *Seismic Provisions for Structural Steel Buildings* (AISC, 2005) do not allow such an approach, however.

Another approach would be to simply ignore the drift and stability limits, and design the system for strength alone. Experience has shown that this approach is not feasible because of the potential for developing large residual displacements, or complete dynamic instability (Ruiz-Garcia and Miranda, 2006). The tendency towards dynamic instability is exacerbated by the low amount of inherent damping that is present in steel systems. It has been recognized that the inherent damping is not likely to be in excess of 2% critical (the almost universal practice of modeling such systems with 5% damping is unconservative).

Finley A. Charney, Professor, Via Department of Civil and Environmental Engineering, Virginia Polytechnic Institute and State University, Blacksburg, VA (corresponding author). E-mail: fcharney@vt.edu

Ozgur Atlayan, Graduate Research Assistant, Via Department of Civil and Environmental Engineering, Virginia Polytechnic Institute and State University, Blacksburg, VA. E-mail: oatlayan@vt.edu

If more damping could be justified the excessive residual deformations and dynamic instabilities might be avoided, and the systems could be designed for strength alone. Exactly such a concept is the focus of the research reported in this paper. It is noted, however, that unlike most of the supplemental damping applications (Miyamoto and Singh, 2002; Hwang, 2002; Miyamoto and Gilani, 2008) that concentrate on the effects of added damping that produce total system damping of 20 to 35% critical, this paper concentrates on adding the minimum amount of damping that is required to obtain an acceptable response. As shown in the remainder of the paper, systems with a total of only 10% damping have the desired performance, with the added benefit of increasing the reliability of the structural system.

VISCOUS FLUID DAMPERS

Viscous fluid dampers include a piston head with orifices contained in a hollow cylinder filled with fluid, which is mostly a compound of silicone or similar type of oil. Energy is dissipated in the damper as the piston rod moves through the fluid and forces the fluid to flow through the orifices in the piston head (Lee and Taylor, 2001). Because the fluid flows at high velocities, it causes friction between fluid particles and the piston head, which produces energy dissipation in the form of heat.

The force–velocity relationship for a viscous fluid damper can be expressed as:

$$F_D = C\left|\dot{u}\right|^{\alpha} \operatorname{sgn}(\dot{u}) \tag{1}$$

where F_D is the damper force, C is the damping constant, $\dot{u}$ is the relative velocity between the ends of the damper, α is an exponent that controls the shape of the force–velocity relationship, and sgn is the signum function used to find the sign of the velocity.

In earthquake engineering, viscous fluid dampers with velocity exponent of 0.3 to 1.0 are typically used (Symans et al., 2008). Using a velocity exponent, α, less than 1.0 causes the dampers to yield at high velocities and thus limits the forces transferred into the structure. When $\alpha = 1.0$, the damper force is proportional to the relative velocity, and the device is called a linear viscous damper.

For a given peak force and displacement amplitude, as the velocity exponent, α, of nonlinear dampers reduces below unity, the area in the force-displacement hysteresis loop gets larger and thus the energy dissipated for a cycle of motion is increased. This behavior is shown in Figures 1 and 2. Figure 1 shows the displacement and velocity histories of an applied sine wave with a period of 1 s. Figures 2a and 2b show the damping force-displacement and damping force-velocity relationships, respectively (as a result of the applied sine wave displayed in Figure 1), for three different C and α values. Note that varying the α value, C was adjusted such that the total damping force is the same (200 kips) for all three dampers. Viscous dampers are attractive from the theoretical viewpoint that velocity is out of phase with the displacement. Forces from viscous dampers will not add to the elastic forces in a structure because the maximum damping

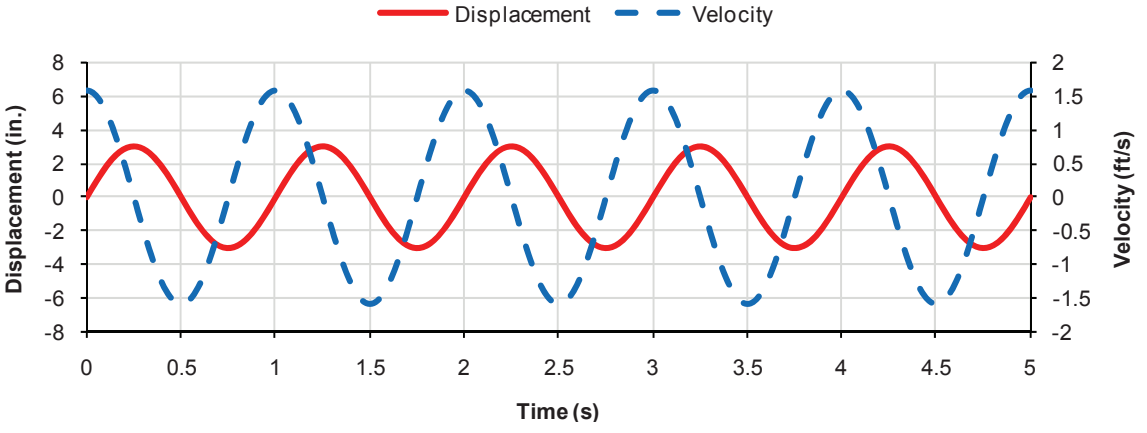

Fig. 1. Phasing of displacement and velocity.

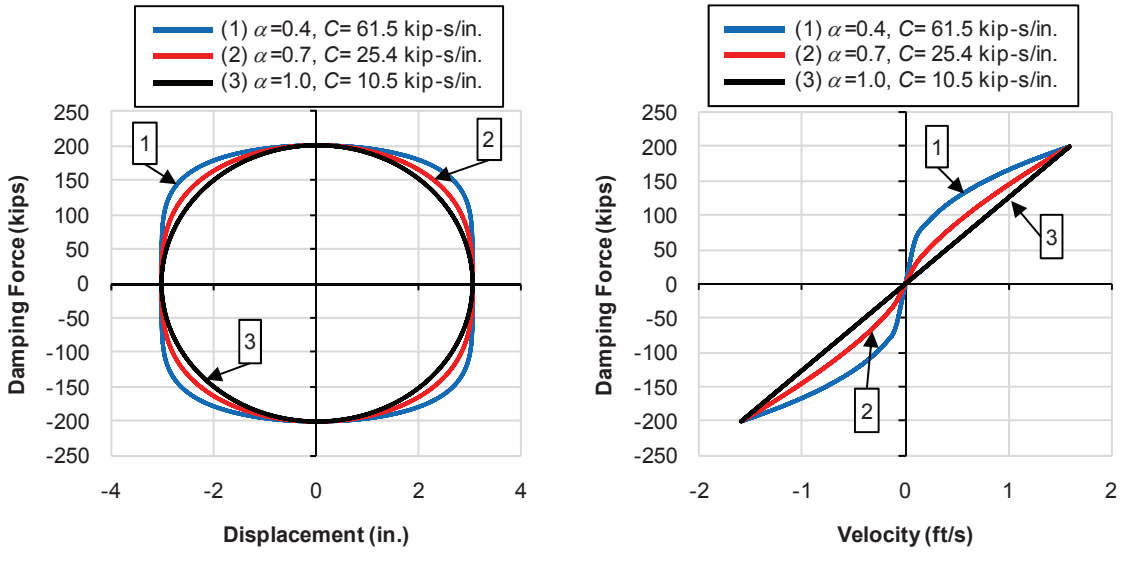

(a) *(b)*

Fig. 2. Damper force-displacement and damper force-velocity relationship for three different dampers.

Table 1. Gravity Loads and Seismic Masses			
Load Type	**Load (psf)**	**Level**	**Mass (kip-s^2/ft)**
Floor dead load	96	Roof	36.55
Roof dead load	83	Floors 2–8	33.93
Penthouse dead load	116	Floor 1	34.52
Exterior wall dead load	25		
Floor/roof reduced live load	20		

forces occur when the elastic forces due to building deformation are small. In practice, however, these two forces do couple to some extent so total force often increases (Kelly, 2001).

The primary advantage of using nonlinear dampers with velocity exponent, α, less than 1.0 is to limit base shears when deformational velocities are large, and the main advantage of using linear dampers is simplified mathematical modeling. In addition, for low-intensity earthquakes, where the structure remains elastic, the damper forces of linear dampers within the story are nearly 90° out of phase with respect to the elastic structural forces. Thus, under certain conditions, the effect of damper forces on the forces at the foundation level will be minimized when linear dampers are used (Symans et al., 2008). In this study, linear viscous dampers with $\alpha = 1.0$ were used.

Dampers can be manufactured to any practically required C and α values. An optimization analysis is required to determine the exact C and α values needed for each damper (Taylor, 2003). In addition, there is always a dilemma between using a large number of small dampers and using a lesser number of large dampers. Architectural restrictions, damper size–cost evaluation, and, obviously, achieving the required structural performance efficiently are important in deciding the number and size of the dampers. Similarly, damper distribution within a structure can be optimized. Wongprasert and Symans (2004) present an optimization technique where frequency-domain objective functions are

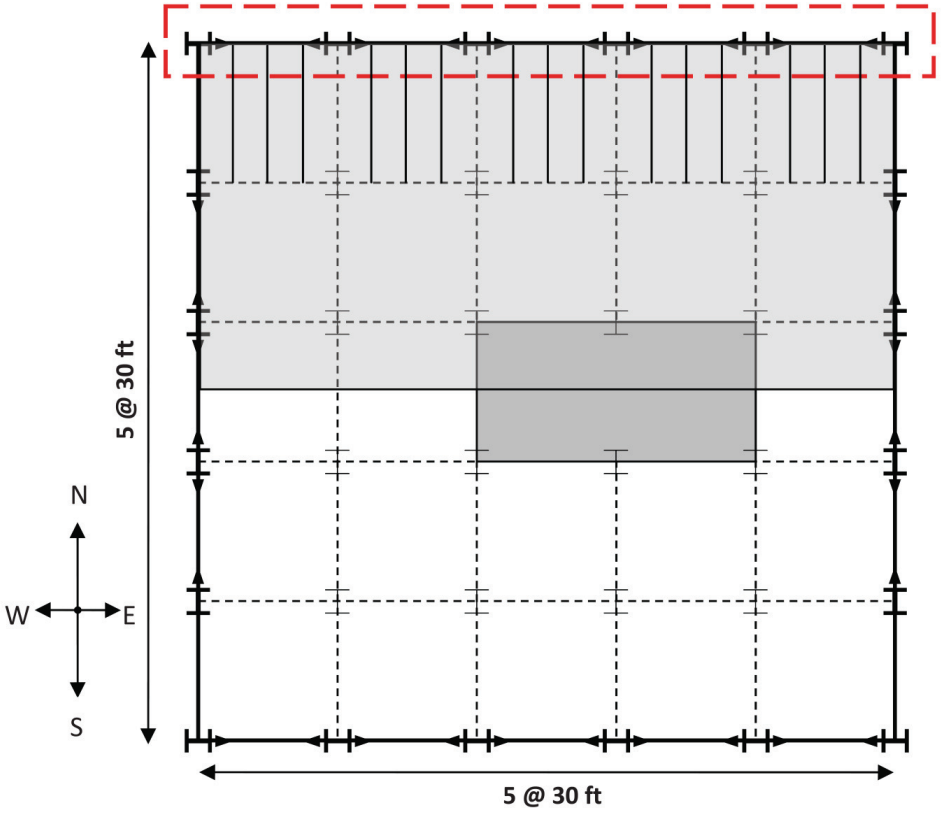

Fig. 3. Plan view of nine-story building.

Table 2. Column and Beam Sections of Strength Controlled Design						
Level	Columns			Beams		
	Exterior	Interior	Middle	Exterior	Interior	Middle
0–1	W18×192	W18×211	W18×192	W27×114	W27×94	W27×94
2–3	W18×130	W18×192	W18×192	W24×103	W24×103	W24×103
4–5	W18×97	W18×158	W18×158	W24×94	W24×94	W24×94
6–7	W18×71	W18×130	W18×130	W24×76	W24×76	W24×76
8–9	W18×50	W18×97	W18×97	W21×62	W21×62	W21×62

Table 3. ASCE 7-05 Design Parameters			
Design Parameter	Value	Design Parameter	Value
0.2 s spectral acceleration, S_S	1.25 g	Seismic Design Category	D
1.0 s spectral acceleration, S_1	0.5 g	Effective seismic weight, W	10,500 kips
Site class	D	Base shear	358 kips
0.2 s design acceleration, S_{DS}	0.83 g	Response modification factor, R	8
1.0 s design acceleration, S_{D1}	0.5 g	Deflection amplification factor, C_d	5.5
Seismic use group	II	Seismic response coefficient, C_S	0.034
Importance factor	1.0	Maximum fundamental period, C_uT_a	1.83 s

considered such that the optimal damper locations are dependent on the building and ground-motion characteristics. In their study, four different objective functions, which have different damper distributions in the structure, are investigated by considering different structural damage measures, and the optimum configuration was decided on the most critical damage measure considered. Note that this optimization was performed under the constraint that the number of dampers and their properties are known parameters.

Dampers can be installed as part of chevron brace, horizontally at top of chevron brace, as diagonal members and as a toggle braced system. In this study, dampers were added horizontally at top of the chevron braces.

MODELS AND DESIGN PROCEDURES

The effect of added viscous fluid dampers was investigated on a five-bay, nine-story steel special moment frame building, located near Seattle, Washington. The building models of the SAC Joint Venture (FEMA, 2000) were used in this study (see Figure 3 for the plan view). The dark gray shaded area in Figure 3 shows the penthouse, and the light gray shaded area shows the total gravity loads applied on the P-delta frame, which will be discussed later. The moment frame used in this study is shown between the dashed lines (E-W direction) in Figure 3. Because two moment frames are used in each lateral direction, each frame resists half of the lateral load in its respective direction. Similar to the SAC Report (FEMA, 2000), it was assumed that sufficient shear resistance is provided between diaphragms and beams so that seismic inertia forces generated at the floor levels can be transferred to the moment frame.

The gravity loads and masses used in this study can be seen in Table 1. The seismic masses shown in Table 1 are for half of the building. Because it is assumed that the loads are carried to the girders with three beams (see Figure 3), the gravity loads were applied as concentrated loads except for the exterior wall dead load, which was applied as a distributed load on the girders of the moment frame.

Strength and Stability Controlled Designs

The purpose of this study was to design a steel moment frame for only strength and then control the drift by using supplemental dampers. Using the mapped acceleration parameters (S_S and S_1), a flexible building design was obtained in Seattle. Because ASCE 7-05 (2006a) permits checking the elastic drift limits by using the lateral forces that are calculated by using the computed period of the structure (instead of the maximum fundamental period at the pre-design stage, C_uT_a), the strength design satisfied the elastic drift requirements of ASCE 7-05 (2006a) under strength-level design earthquake forces. Although the strength-controlled design met the drift requirements, the stability checks (due to P-delta effects) of both ASCE 7-05 and the Commentary to the 2005 AISC *Seismic Provisions* were not satisfied. Using the stability checks of ASCE 7-05 and the seismic provisions Commentary, another moment frame was designed with increased member sizes at the lower levels. Thus, two different nine-story special moment

frames (SMFs) were designed in Seattle, called the stability-controlled and strength-controlled designs. See Table 2 for the column and beam sections of the strength-controlled design for which added dampers will be implemented.

The computed periods for stability-controlled and strength-controlled designs were 3.19 and 3.29 s, respectively. The computed period values were more than expected for a nine-story building. The calculated period in the SAC report (FEMA 2000), for the nine-story building in Seattle, is between 3.06 and 3.17 s, depending on the panel zone modeling. However, periods vary between 2.20 and 2.40 s for a nine-story building in Los Angeles in the same report. The reason for the different periods in Los Angeles is the high demands, due to different S_S and S_1 parameters, which result in a stiffer structure. Thus, it was concluded that the calculated high-period values were reasonable and related with the regional seismic parameters of Seattle. The ASCE 7-05 design parameters used for the designs are summarized in Table 3.

To move the plastic hinges away from the column face, reduced beam sections were used, and the moment rotation properties of each hinge, forming at the reduced sections, were calculated explicitly (Atlayan, 2008). Panel zones were represented by use of Krawinkler's model (Charney and Marshall, 2006). See Atlayan (2008) for a much more detailed description of the step-by-step procedures of beam, column and panel zone design and differences between the stability and strength designs.

P-delta Effects and Damping Modeling

P-delta effects were included in all analyses using a special linear P-delta frame, shown at the right of Figure 4. This frame, sometimes called a ghost column or a leaner column, is needed in two-dimensional analysis because the gravity load tributary to the moment frames (and used for strength design of the frames) is significantly less than the destabilizing gravity load on the system.

All structures have the ability to dissipate energy during free vibration. This energy loss is generally referred as inherent damping. The main sources of inherent damping are material damping due to internal stresses, cracking in the structural materials, and friction in the connections and in the nonstructural components (Charney, 2008). A separate frame, shown to the left in Figure 4, was used to model the inherent damping. Similar to the P-delta frame, the inherent damping frame was laterally constrained to the main structural system. The reason for using the inherent damping frame was to provide an explicit control over the damping in the system.

Inherent damping was calculated by using Rayleigh damping. The total damping in each structure was determined by

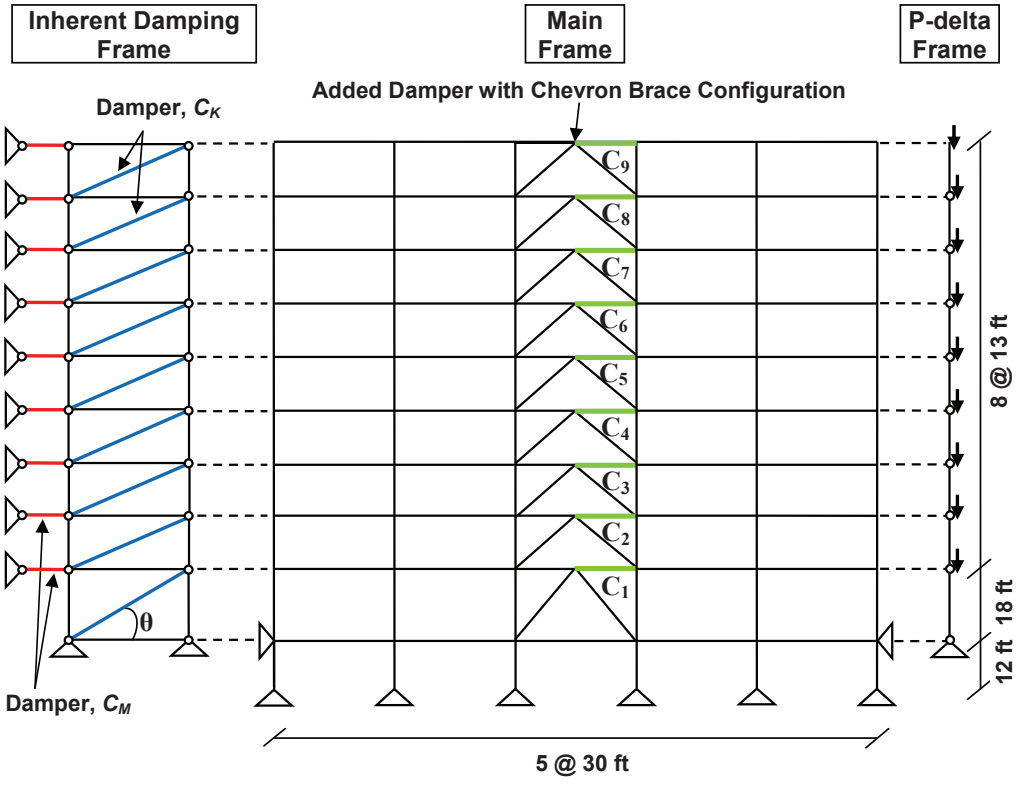

Fig. 4. Inherent damping and P-delta frames constrained to main frame.

Table 4. Inherent and Added Damping Coefficients for Stability and Strength Controlled Designs				
	Strength-Controlled Design		Stability-Controlled Design	
	Mass Proportional Constant	Stiffness Prop. Constant	Mass Proportional Constant	Stiffness Prop. Constant
	$\alpha = 0.071868$	$\beta = 0.001200$	$\alpha = 0.073938$	$\beta = 0.001198$
Story	C_M (kip-s/in.)	C_K (kip-s/in.)	C_M (kip-s/in.)	C_K (kip-s/in.)
9th story	0.219	0.499	0.226	0.495
8th story	0.203	1.035	0.209	1.032
7th story	0.203	0.949	0.209	0.945
6th story	0.203	1.344	0.209	1.346
5th story	0.203	1.292	0.209	1.291
4th story	0.203	1.646	0.209	1.645
3rd story	0.203	1.720	0.209	1.720
2nd story	0.203	1.962	0.209	2.104
1st story	0.207	1.036	0.213	1.256
Damping coefficient for 5% total damping (same at each story)	12.57			
Damping coefficient for 10% total damping (same at each story)	35.62			

setting the critical damping ratio to 2% at the natural period of the structure and at a period of 0.2 s. Using mass proportional constant α and stiffness proportional constant β, the desired level of inherent damping (2% of critical) was achieved. The damping coefficients C_M and C_K were calculated by using the following formulas at each story:

$$C_M = \alpha M_x \tag{2}$$

$$C_K = \beta K_x / \cos^2(\theta) \tag{3}$$

where M_x is the total story mass and K_x is the total story stiffness. The virtual work method was used to find the story stiffnesses. Because the stiffness proportional dampers were used in a diagonal configuration, the damping coefficients were modified using the angle between the braces and the horizontal plane to account for the effective reduction of the diagonal damper, as shown in Equation 3. The stiffness and mass damping coefficients in Table 4 (without added dampers) provide 2% inherent damping when assigned to the inherent damping frame for the corresponding strength or stability controlled designs.

Added Dampers

In order to increase the total system damping, viscous fluid dampers were added to the strength-controlled frame, producing two additional frames, which will be called the 5% and 10% total damped strength designs. These dampers represent physical linear viscous fluid damping devices that would be incorporated into the structural system.

The added damping coefficients were found by using the modal strain energy tools that are included in the NONLIN-Pro computer program (Charney and Barngrover, 2006). The added damper coefficients were updated until the total damping of the strength design reached 5 and 10% of critical. The added dampers were distributed equally at each story, and a chevron brace configuration was used to support the dampers, as shown in Figure 4. The chevron brace configuration was used to provide complete control over the modeling of inherent damping and thereby avoid the potentially adverse consequences of modeling inherent damping as a viscous mechanism (Charney, 2008). See Table 4 for the damping coefficients used in this study.

ANALYSIS OF A NINE-STORY MOMENT-RESISTING STEEL FRAME WITH AND WITHOUT ADDED DAMPERS

Two types of analysis were performed for each frame: nonlinear static pushover analysis (NSP) and incremental dynamic analysis (IDA). All structural analyses were conducted using Perform-3D (CSI, 2006). A planar model consisting of one of the two perimeter frames (E-W direction), which are parallel to the design ground motion, was used.

Nonlinear Static Pushover Analysis

Figure 5 displays the nonlinear static pushover curves with highlighted target displacements, first significant yields and the design base shear for both of the designs. Both models were pushed up to 4% reference drift, which is twice the drift limit of ASCE 7-05.

First significant yield is the level of force that causes the formation of the first plastic hinge in the structure, and the design base shear is $V = C_s W$, where C_s is the seismic response coefficient and W is the weight of the structure. The reason for the difference among the design base shear, first significant yield and actual strength of the structure is the overstrength. The overstrength factor is the ratio of the apparent strength to the design strength. As can be seen from the pushover curves, the overstrength factor was about 2 for the stability-controlled design and about 1.85 for the strength-controlled design. The reasons for the overstrength are the sequence of yielding of critical regions, load factors on the gravity system, strain hardening, capacity reduction (ϕ) factors and member selections (strong column–weak beam). Note that the system overstrength factor for special moment frame, Ω_0, is 3 in ASCE 7-05. Also, Ω_0 is not a true overstrength but an upper bound used for proportioning vulnerable components. Thus, Ω_0 is not used to assess the true system overstrength.

Both pushover curves reach negative stiffness due to the P-delta effects. Because the strong column–weak beam rule is satisfied in both of the designs, the only plastic hinges that formed in the columns formed at the bottom of the first story, when the structures were pushed up to the target displacement. Thus, weak-story mechanisms did not occur up to the target displacement level of pushover analyses.

The target displacement, which is intended to represent the maximum displacement likely to be experienced during the design earthquake, was found using the procedures outlined in ASCE 41-06 (2006b). If the stability ratios of the stories are more than the limit stipulated in ASCE 7-05, it is advisable to check the post-yield slope of the pushover curve at the target displacement and determine whether or not that slope is positive or negative. Note from Figure 5 that the tangent stiffness of the pushover curve is positive at the target displacement for the stability-controlled design, whereas the tangent stiffness of the strength-controlled design becomes negative prior to reaching the target displacement. This is an early warning for the possible collapses of the strength-controlled design without added dampers.

Incremental Dynamic Analysis

In this study, incremental dynamic analysis (Vamvatsikos, 2002) was conducted by using 10 different earthquake records with intensities of 0.2 to 2.0 times the ground motion scaled to match the design basis earthquake. Thus, the scale factor of 1.0 corresponds to the design basis earthquake (DBE), and the scale factor of 1.5 corresponds to the maximum considered earthquake (MCE). The ground motions were initially scaled to match the ASCE 7-05 spectrum at the structure's fundamental period. This scaling procedure was recommended for IDA analysis by Shome et al. (1998). The ground motions used in the analysis were the same as those used in the original SAC research (FEMA, 2000),

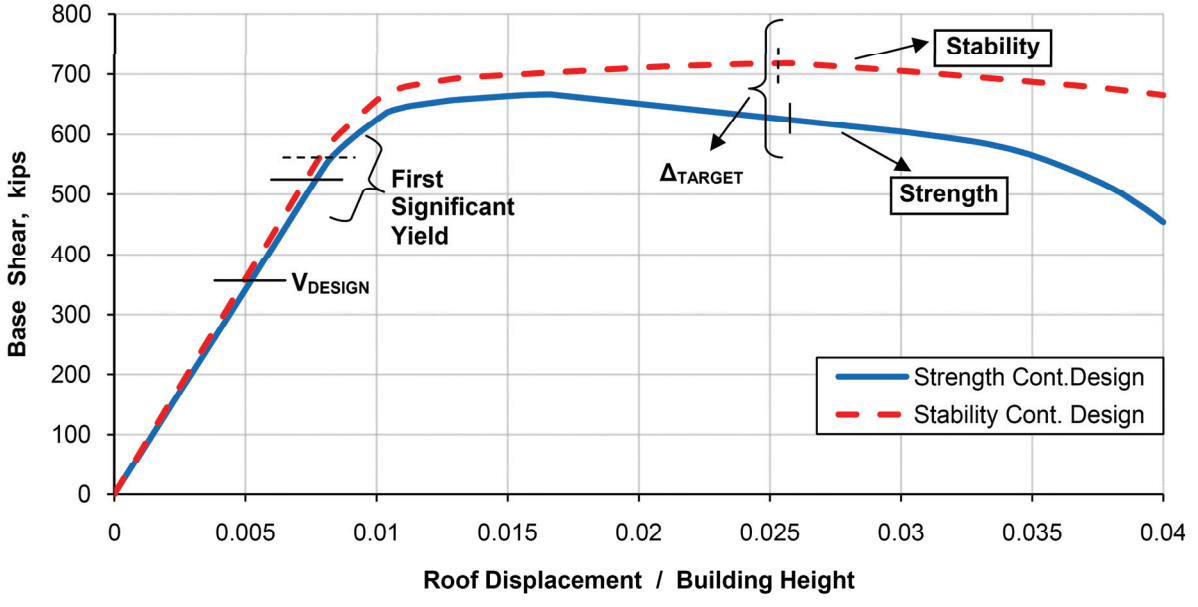

Fig. 5. Nonlinear static pushover curves for strength and stability controlled designs.

Table 5. Ground Motions							
Earthquake No.	SAC Name	Earthquake Name	Magnitude	Duration (s)	Time Step (s)	PGA (g)	Integration Time Step (s)
EQ00	SE 21	Mendocino, 1992	7.1	59.980	0.020	0.771	0.005
EQ01	SE 23	Erzincan, 1992	6.7	20.775	0.005	0.476	0.005
EQ02	SE 25	Olympia, 1949	6.5	79.980	0.020	0.206	0.005
EQ03	SE 27	Seattle, 1965	7.1	81.820	0.020	0.175	0.001
EQ04	SE 29	Valparaiso 1, 1985	8.0	99.975	0.025	0.564	0.0025
EQ05	SE 31	Valparaiso 2, 1985	8.0	99.975	0.025	0.321	0.001
EQ06	SE 33	Deep Interplate	7.9	79.980	0.020	0.207	0.001
EQ07	SE 36	Miyagi-oki, 1978	7.4	79.980	0.020	0.440	0.001
EQ08	SE 37	Shallow Interplate 1	7.9	79.980	0.020	0.599	0.005
EQ09	SE 40	Shallow Interplate 2	7.9	79.980	0.020	0.503	0.001

which are shown in Table 5. Bracketed duration, the time interval between the first and the last occurrence of an acceleration of 0.05 g, was calculated for each ground motion and used to establish the computation time of the analyses.

To prevent the numerical errors and fictitious dynamic instability, Newmark integration time steps were checked for each ground motion. The roof displacement response history was checked with the ground motions that have a scale factor of two times the DBE. In other words, the response histories of the roof were evaluated with the largest scale factor that does not cause collapses in the IDA study, and the time step was decreased by half of the previous one until the responses converged. In addition, each time a collapse occurred, the reasons for dynamic instabilities were investigated explicitly to differentiate the real collapses from numerical errors.

For the IDA study, the scale factor of the ground motions was used as the intensity measure, and the interstory drift, base shear, maximum and residual roof displacements, and IDA dispersion were used as the damage measures.

Effect of Dampers on Drift

As discussed earlier, the elastic drift limits of ASCE 7-05 were satisfied for both of the inherently damped strength and stability designs. In addition to the elastic drift limit

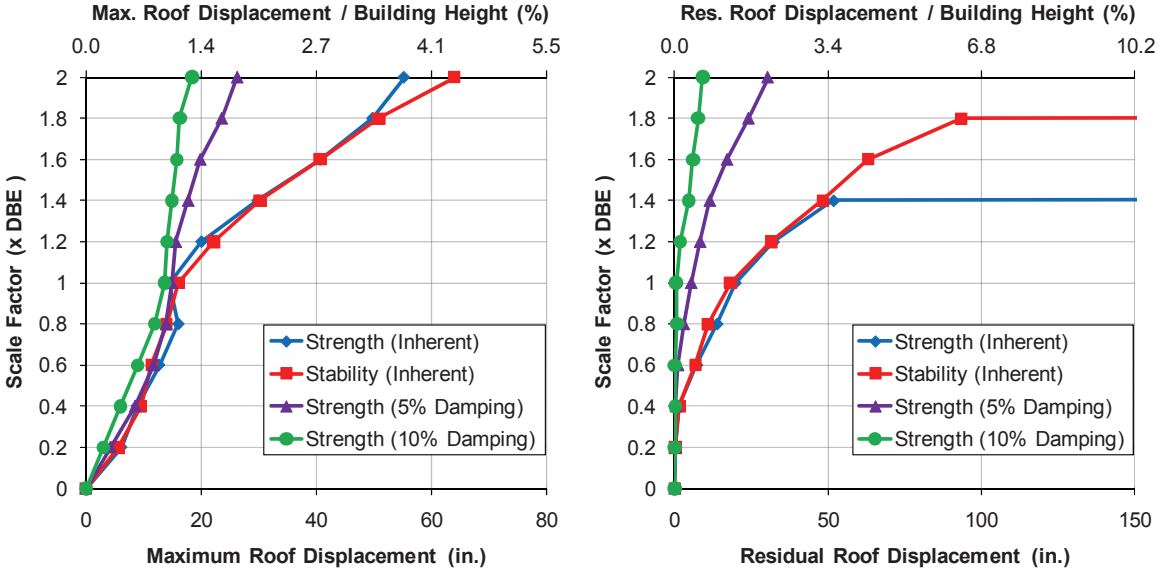

(a) *(b)*

Fig. 6. IDA plots for maximum and residual roof displacements using (a) Valpariso-1 and (b) Seattle ground motions.

Table 6. Maximum Drifts for Design Basis Miyagi-oki and Valparaiso-2 Earthquakes									
Level	Drift Limit (%125) (in.)	Miyagi-oki				Valparaiso-2			
		Strength Inherent Damping (in.)	Stability Inherent Damping (in.)	Strength 5% Damping (in.)	Strength 10% Damping (in.)	Strength Inherent Damping (in.)	Stability Inherent Damping (in.)	Strength 5% Damping (in.)	Strength 10% Damping (in.)
9th	3.90	3.13	3.37	1.94	1.02	**5.00**	**5.41**	2.21	1.04
8th	3.90	3.59	**4.16**	2.63	1.52	**6.64**	**7.61**	3.15	1.64
7th	3.90	**4.53**	**4.96**	2.97	1.99	**4.97**	**5.46**	3.37	1.98
6th	3.90	**4.46**	**4.81**	3.33	2.40	**4.06**	**5.28**	2.90	2.07
5th	3.90	**4.08**	**4.75**	3.37	2.69	**4.24**	**5.49**	2.73	2.02
4th	3.90	**4.36**	**4.74**	3.47	2.99	3.22	3.67	3.01	2.07
3rd	3.90	**4.64**	**4.63**	3.49	3.16	2.84	3.42	3.09	2.18
2nd	3.90	**4.30**	3.53	3.54	3.19	2.77	3.11	2.92	2.35
1st	5.40	**5.40**	4.04	4.12	3.69	4.63	4.37	3.56	3.01

check, according to Chapter 16 of ASCE 7-05, the results of nonlinear response history analysis (NRHA) shall not exceed 1.25 times the allowable drift limit (2% of story height in this study). However, the results of NRHA exceeded 1.25 times the allowable drift limit for both of the inherently damped designs for 6 out of 10 earthquakes used in this study. The added dampers play a crucial role here. Table 6 shows the maximum drift results of all the designs subject to two different ground motions at the design level. Note that the highlighted values exceed the limits.

For this study, the 5% totally damped strength controlled design satisfied the drift requirements under all 10 different earthquakes used. As expected, a further decrease in drift values occurred when the total damping increased to 10% of critical. Thus, a structure that satisfies the elastic drift limits of the code may not satisfy the drift limits by NRHA, but these limits can be met by using supplemental damping.

Figures 6a and 6b illustrate the maximum and residual roof displacement IDA plots by using the Valpariso-1 and Seattle earthquakes, respectively. All the designs resisted Valpariso-1 earthquake. However, the inherently damped strength design collapsed after the scale factor of 1.4 times the DBE, and the stability design collapsed after the scale factor of 1.8 times the DBE when frames are subjected to Seattle earthquake. Note that horizontal lines in IDA curves indicate collapses (see Figure 6b). The frames with added

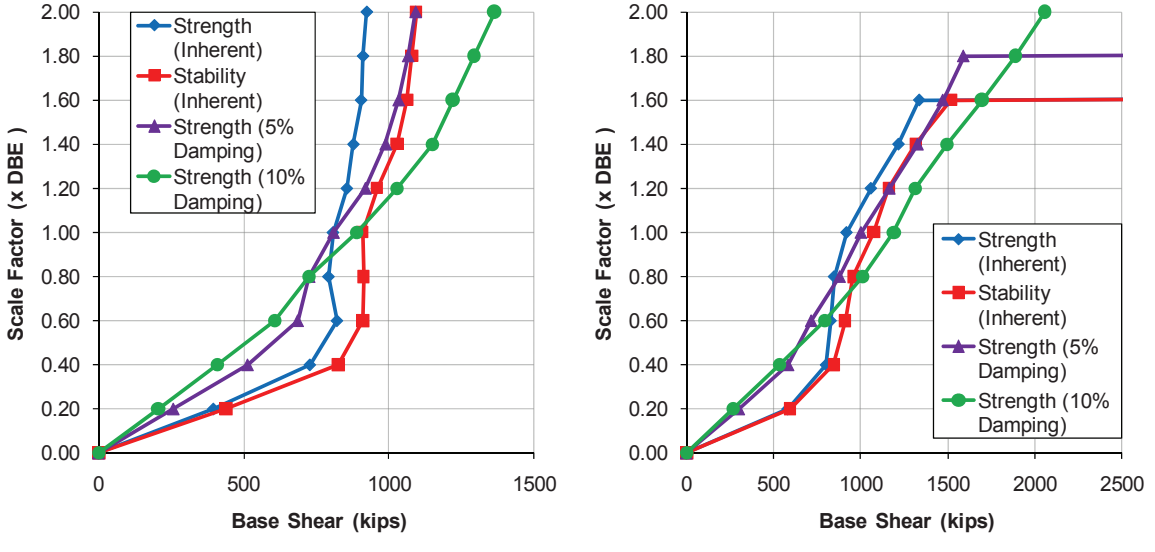

(a) *(b)*

Fig. 7. Base shear IDA plots for (a) Erzincan and (b) Miyagi-oki earthquakes.

dampers resisted the collapses for Seattle earthquake and reduced the maximum and residual roof displacements significantly.

Effect of Dampers on Base Shear

Figures 7a and 7b display base shear IDA plots for the Erzincan and Miyagi-oki earthquakes. At low-scale factors, where the structure behaves elastically, base shear decreases as damping increases. The IDA curves generally intersect before displaying an increase in terms of base shear with increased damping in the nonlinear region. The 5% damped strength-controlled design and the inherently damped stability-controlled design behaved very similar in base shear IDA responses after the structures yield. This is particularly true at ground-motion levels approaching the design and maximum considered earthquakes (scale factors 1.00 and 1.50, respectively). The same behavior was observed for the other eight earthquakes used in this study as well. Note that the difference between the base shear IDA plots of stability and 5% damped strength designs (at scale factors more than 1.60) in Figure 7b was due to collapses. The inherently damped stability design collapsed when the

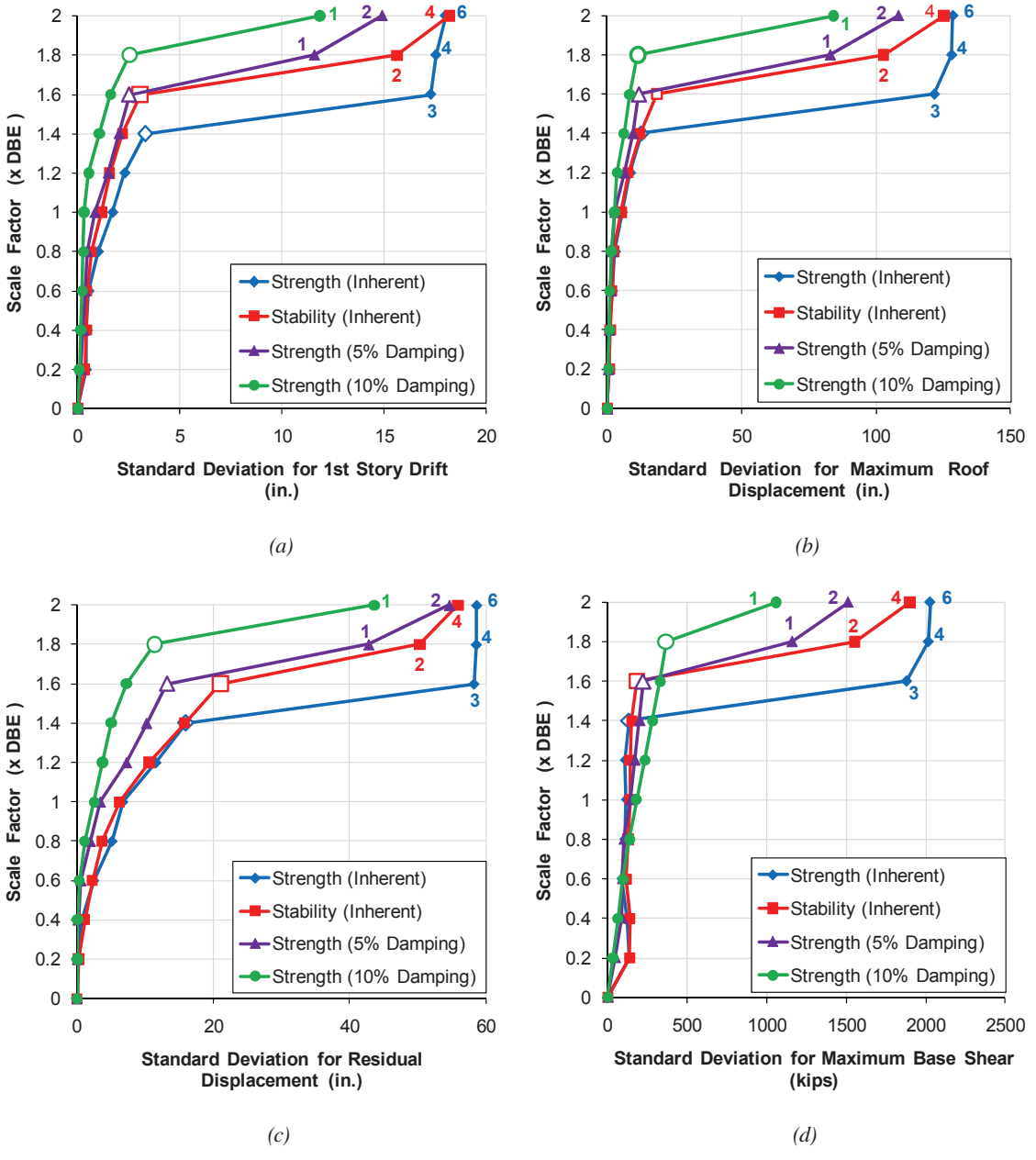

Fig. 8. Standard deviation IDA plots for different damage measures.

scale factor reached 1.80; however, the 5% damped strength design resisted the scale factor 1.80 and collapsed at a factor of 2.00 when the frames were subjected to Miyagi-oki earthquake.

The main drawback of linear viscous dampers is the high base shears in the inelastic region of the IDA plots. This study concludes that 5% damping with linear viscous dampers does not cause base shear problems. The 10% total damping increases the base shear between 10 and 30%, depending on the earthquake. As discussed earlier, the use of nonlinear viscous dampers, with the velocity exponent of about 0.4, would likely reduce the increase in base shear associated with added viscous damping, but this was not investigated in this study.

Effect of Dampers on IDA Dispersion

The dispersion of IDA curves can be used to see the effect of dampers in terms of giving a reliable estimate of the performance of the buildings. To measure the IDA dispersion, the standard deviation of the responses, produced at each intensity level of 10 different earthquakes, was calculated for each structure with different amounts of damping. The standard deviation increases as the amount of dispersion increases. When the standard deviation IDA curves for the different levels of damping are displayed together, the curve that has the steepest slope will correspond to the system that is best at reducing the IDA dispersion.

Figures 8a through 8d illustrate the IDA dispersion for different damage parameters. While the building response is elastic, there was not a significant dispersion. As the earthquake intensity increased, dispersion increased as well, and when the buildings collapse, dispersion increased because of the collapse measures used for the dispersion study. In all of the dispersion plots, the horizontal lines occurring at high-intensity measures indicate the collapses. The number of earthquakes that caused collapse is also labeled at the corresponding scale factors. Note that the final scale factors that resisted the collapses of all earthquakes are shown with an unfilled (empty) data point in Figure 8. When IDA dispersion plots are analyzed, it can be concluded that the 10% total damped strength-controlled design had a drastically improved performance when compared to the other designs. The 10% damped strength design gave higher dispersion or uncertainty than the other designs only for the base shear damage measure between scale factors of 0.8 and 1.6 (see Figure 8d). This was an expected result if the drawback of the linear viscous dampers at high damping ratios was considered. Above the scale factor of 1.6, the 10% damped strength design gave better results in terms of base shear IDA dispersion as well, because the other designs collapsed at high earthquake intensities and the use of collapse measures increased the dispersion.

Effect of Dampers on Energy Dissipation

Dampers reduce the damage in the structure by dissipating energy. Figures 9, 10 and 11 respectively illustrate the

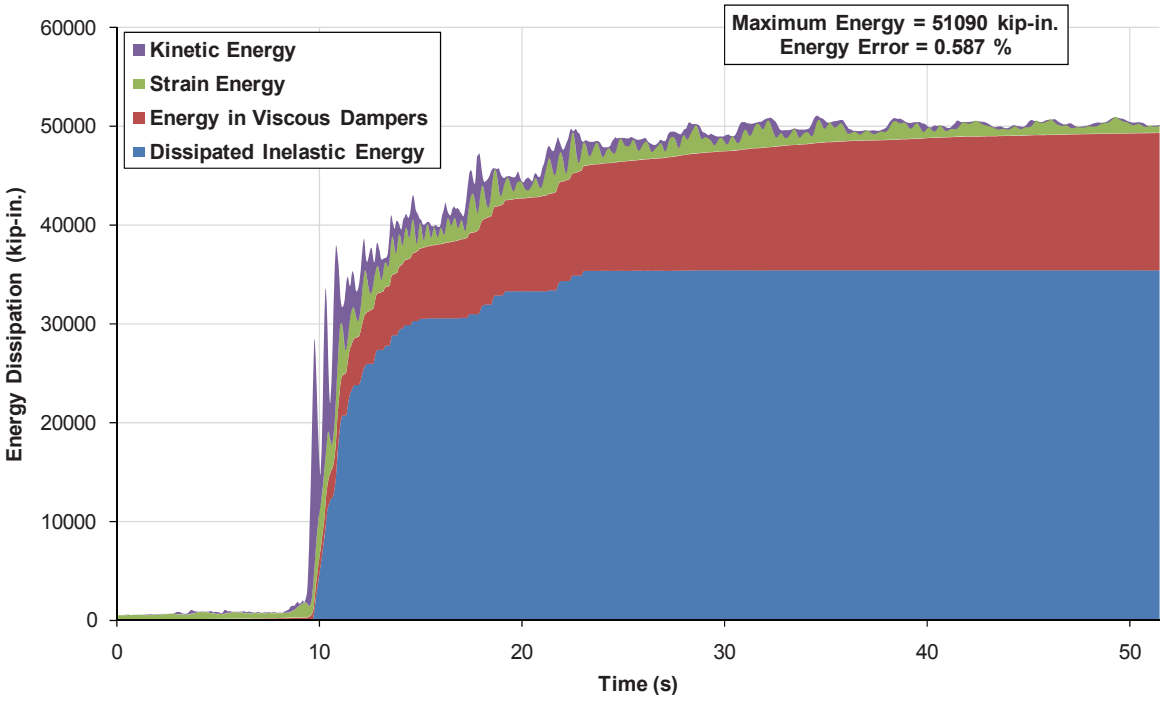

Fig. 9. Energy balance plot for inherently damped strength design frame under EQ07 (DBE).

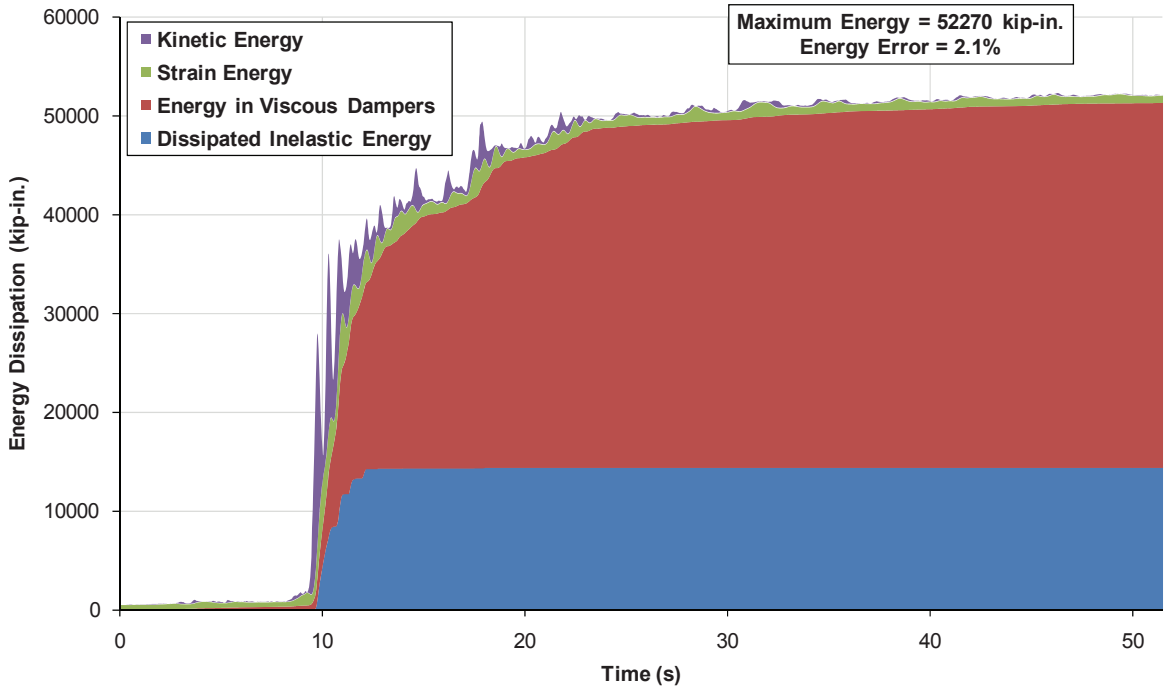

Fig. 10. Energy balance plot for 5% total damped strength design frame under EQ07 (DBE).

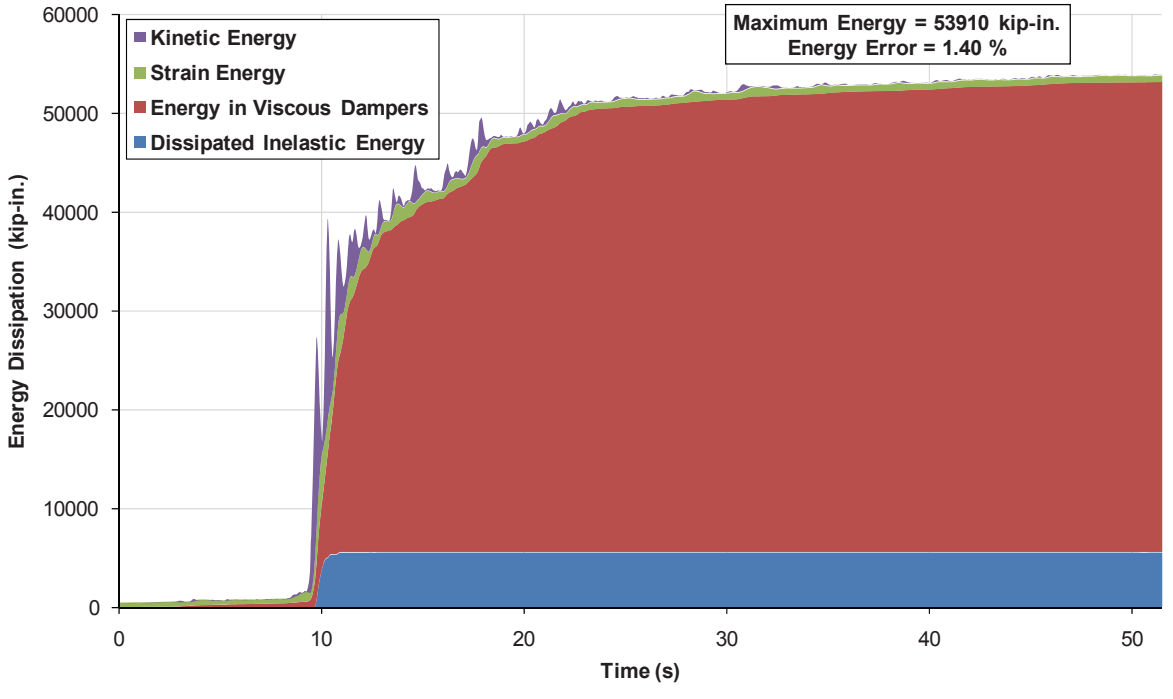

Fig. 11. Energy balance plot for 10% total damped strength design frame under EQ07 (DBE).

Table 7. Collapse Check for Selected Earthquakes							
Design	**Scale Factor**	**Seattle**	**Valparaiso-2**	**Deep Interpolate**	**Miyagi-oki**	**Shallow Interpolate-1**	**Shallow Interpolate-2**
Strength-controlled design with inherent damping	1.0	√	√	√	√	√	√
	1.2	√	√	√	√	√	√
	1.4	√	√	√	√	√	√
	1.6	Collapse	Collapse	√	√	√	Collapse
	1.8	Collapse	Collapse	√	Collapse	√	Collapse
	2.0	Collapse	Collapse	Collapse	Collapse	Collapse	Collapse
Stability-controlled design with inherent damping	1.0	√	√	√	√	√	√
	1.2	√	√	√	√	√	√
	1.4	√	√	√	√	√	√
	1.6	√	√	√	√	√	√
	1.8	√	√	√	Collapse	√	Collapse
	2.0	Collapse	Collapse	√	Collapse	√	Collapse
Strength-controlled design with 5% total damping	1.0	√	√	√	√	√	√
	1.2	√	√	√	√	√	√
	1.4	√	√	√	√	√	√
	1.6	√	√	√	√	√	√
	1.8	√	√	√	√	√	Collapse
	2.0	√	√	√	Collapse	√	Collapse
Strength-controlled design with 10% total damping	1.0	√	√	√	√	√	√
	1.2	√	√	√	√	√	√
	1.4	√	√	√	√	√	√
	1.6	√	√	√	√	√	√
	1.8	√	√	√	√	√	√
	2.0	√	√	√	√	√	Collapse

energy plots when the inherently 5% and 10% damped strength designs were subjected to Miyagi-oki earthquake (EQ07). These plots show how the ground-motion input energy is dissipated and absorbed by the structural system. In the energy plots, the X-axis is time and the Y-axis is the amount of different energy types in the system at the given time. As can be seen from the energy plots, as the damping increased (moving from Figure 9 to Figure 10 to Figure 11), the energy dissipated by viscous damping (inherent plus added damping) increased, and the dissipated inelastic energy decreased. Thus, structural damage decreased because this damage is related directly to dissipated inelastic energy. Strain and kinetic energy ratios are also shown in the energy plots. The energy errors shown in the plots are a measure of the accuracy of the structural analysis. The maximum error of 2.1 percent shown in Figure 10 is somewhat higher than desired but is acceptable for the purposes of this study.

Effect of Dampers on Dynamic Instability

One of the main purposes of this study was to investigate the effect of added dampers on dynamic instability (collapses). Table 7 shows the collapse check of the four structures subject to six earthquakes, from scale factors 1.0 to 2.0, which caused collapses in the IDA studies. Both the strength- and the stability-controlled designs did not collapse until the MCE. However, the strength design collapsed just after the MCE for three earthquakes, when the IDA scale factor reached 1.6. The main collapse mechanism was the intermediate-story mechanisms occurring at the bottom three stories due to P-delta effects.

The effect of damping on dynamic instability was obviously significant. Five percent damping prevented the collapses of four out of six earthquakes that occurred in the strength-controlled design. The 10% total damped structure resisted all the earthquakes except EQ09 with scale factor

of 2.0. The amount of damping necessary to prevent the collapse was dependent on the design of the structure. Regarding the strength-controlled design investigated in this study, 10% total damping was conservatively adequate for providing dynamic stability.

Note that the stability-controlled design (inherently damped) eliminated half of the collapses that occurred for the inherently damped strength-controlled design. This is consistent with the results of nonlinear pushover analyses. Because strength-controlled design reached negative stiffness before target drift on the pushover curve, story mechanisms and then collapses occurred at MCE level of shaking, which is almost the same level as a 1.6 scale factor in IDA studies.

CONCLUSIONS

The supplemental dampers have a remarkable effect on reducing the inelastic response of the elements of steel moment frames. The effects of added dampers were studied through incremental dynamic analysis by using various damage measures. After adding the linear viscous dampers to the strength designed frame, a significant performance improvement was achieved. The IDA responses of the roof displacement, residual displacement and interstory drifts decreased drastically as a result of added dampers. Although the inherently damped strength design satisfied the elastic drift requirements of ASCE 7-05, it did not meet the drift requirements for the nonlinear response history procedure where the allowable drift limits were increased by 25%. However, after adding the dampers, 5% total damping was adequate to meet the drift criteria of ASCE 7-05.

A collapse check study and an IDA dispersion study were implemented to investigate the effect of damping on dynamic instability. Regarding the optimum level of damping, 5% total damping was almost always adequate to prevent collapse at the MCE level. As the damping increased, the IDA dispersion plots got steeper, which indicates a more reliable performance of the structure under various earthquakes. The 10% total damped strength design gave the best results, followed by 5% damped strength and stability designs, in terms of IDA dispersion.

If the overall performance of the building under different damage measures used in IDA study is considered, the strength-controlled design with 10% damping is concluded to be efficient for the nine-story SMF building in Seattle, Washington. The required level of total system damping might vary for different type of steel frames at other locations; however, it is foreseen that the design approach discussed in this paper is worth consideration in addition to the conventional design methods for moment frame structures in highly seismic regions.

REFERENCES

AISC (2005), *Seismic Provisions for Structural Steel Buildings*, ANSI/AISC 341-05, American Institute of Steel Construction, Chicago, IL.

ASCE (2006a), *Minimum Design Loads for Buildings and Other Structures*, ASCE/SEI 7-05, American Society of Civil Engineers, Reston, VA.

ASCE (2006b), *Seismic Rehabilitation of Existing Buildings*, ASCE/SEI 41-06, American Society of Civil Engineers, Reston, VA.

Atlayan, O. (2008), "Effect of Viscous Fluid Dampers on Steel Moment Frames Designed for Strength, and Hybrid Steel Moment Frame Design," M.S. Thesis, Department of Civil Engineering, Virginia Tech, Blacksburg, VA, http://scholar.lib.vt.edu/theses/available/etd-05072008-110653/.

Charney, F.A. (2008), "Unintended Consequences of Modeling Damping in Structures," *Journal of Structural Engineering*, ASCE, Vol. 134, pp. 581–592.

Charney, F.A. and Barngrover, B. (2006), *NONLIN-Pro Base Program Description and User's Guide*, Advanced Structural Concepts Inc., Blacksburg, VA.

Charney, F.A. and Marshall, J.D. (2006), "A Comparison of the Krawinkler and Scissors Models for Including Beam-Column Joint Deformations in the Analysis of Steel Frames," *Engineering Journal*, AISC, Vol. 43, No. 1, pp. 31–48.

CSI (2006), *Perform-3D User's Guide*, Nonlinear Analysis and Performance Assessment of Structures, Computers and Structures Inc., Berkeley, CA.

FEMA (2000), *State of the Art Report on Systems Performance*, FEMA-355C, Federal Emergency Management Agency, Washington, DC.

Hwang, J.S. (2002), "Seismic Design of Structures with Viscous Dampers," International Training Program for Seismic Design of Building Structures, National Center for Research on Earthquake Engineering of Taiwan, http://www.ncree.gov.tw/itp2002/.

Kelly, T.E. (2001), *In Structure Damping and Energy Dissipation*, Design Guidelines, Holmes Consulting Group Ltd, Wellington, New Zealand.

Lee, D. and Taylor, D.P. (2001), "Viscous Damper Development and Future Trends," *The Structural Design of Tall Buildings*, Vol.10, No. 5, pp. 311–320.

Miyamoto, H.K. and Gilani, A. (2008), "Design of a New Steel-Framed Building Using ASCE 7 Damper Provisions," *Proc. 2008 Structures Congress,* Vancouver, BC, Canada, pp. 1–10.

Miyamoto, H.K. and Singh, J.P. (2002), "Performance of Structures with Passive Energy Dissipators," *Earthquake Spectra*, Vol. 18, No. 1, pp. 105–119.

Ruiz-Garcia, J. and Miranda, E. (2006), "Evaluation of Residual Drift Demands in Regular Multi-Story Frames for Performance Based Seismic Assessment," *Earthquake Engineering and Structural Dynamics*, Vol. 35, No. 13, pp. 1609–1629.

Shome, N., Cornell, C.A., Bazzurro, P. and Carballo, J.E. (1998), "Earthquakes, Records and Nonlinear Responses," *Earthquake Spectra*, Vol. 14, pp. 469–500.

Symans, M.D., Charney F.A., Whittaker A.S., Constantinou M.C., Kircher C.A., Johnson M.W. and McNamara R.J. (2008). "Energy Dissipation Systems for Seismic Applications: Current Practice and Recent Developments," *Journal of Structural Engineering*, ASCE, Vol. 134, pp. 3–21.

Taylor, D.P. (2003), "Mega Brace Seismic Dampers for the Torre Mayor Project at Mexico City," Taylor Devices Inc., NY, http://www.taylordevices.eu/case-studies.php.

Vamvatsikos, D. (2002), "Seismic Performance, Capacity, and Reliability of Structures as Seen Through Incremental Dynamic Analysis," Ph.D. Thesis, Department of Civil Engineering, Stanford University, Stanford, CA.

Wongprasert, N. and Symans, M.D. (2004), "Application of a Genetic Algorithm for Optimal Damper Distribution within the Nonlinear Seismic Benchmark Building," *Journal of Engineering Mechanics*, ASCE, Vol. 130, No. 4, pp. 401–406.